Grain-boundary diffusion of cation vacancies in nickel oxide: A molecular-dynamics study

Theodoros Karakasidis and Madeleine Meyer
Laboratoire des Solides Irradiés, CNRS URA 1380, CEA/DTA/CEREM/DECM, École Polytechnique, F91128 Palaiseau Cedex, France
(Received 29 July 1996)

The diffusion of doubly charged nickel vacancies in a $\Sigma5(310)[001]$ tilt grain boundary (GB) of NiO has been studied by molecular dynamics. The simulations are carried out in the NVT ensemble (constant number of particles, volume, and temperature) and the interatomic interactions are described by a rigid ion potential. The analysis of the atomic trajectories shows that the diffusion of the vacancies occurs by jumps between first-neighbor sites. The migration path only involves a restricted number of sites in the GB and the residence times of the vacancy on the most frequently visited sites have been computed. There is no direct relation between the frequencies of visits and the vacancy formation energies calculated for these sites. We have calculated the vacancy jump frequencies and deduced the diffusion coefficient of this defect at high temperature. The vacancy diffusion is slightly faster along the direction parallel to the GB tilt axis than in the perpendicular direction. The value of this anisotropy is consistent with the experimental results obtained for other oxides. The bulk diffusion of the nickel vacancy has been investigated with simulations performed in a perfect crystal. A qualitative analysis of the atomic trajectories shows that the nickel diffusion is enhanced at the boundary. The GB diffusion enhancement has been quantitatively estimated and compared to the experimental results. [S0163-1829(97)05720-2]

I. INTRODUCTION

Grain-boundary (GB) diffusion is of importance in the processing of ceramic materials as well as in metal oxidation. It is generally established that the grain boundaries are short circuits for diffusion and thus they can play an important role in all the diffusion-dependent properties of materials such as creep, sintering, corrosion, and ionic conductivity. The effect of the grain boundaries is particularly noticeable at relatively low temperatures where the bulk diffusion is less important.

The grain-boundary diffusion has been studied experimentally in some oxides and particularly in those that have an NaCl structure, such as NiO and MgO. The experimental results do not supply a detailed description of the diffusion at a microscopic level. This is a domain where computer simulations can provide useful insight; but up to now there have been very few dynamic simulations of grain-boundary diffusion in ionic materials. In the case of oxides, the computations are limited to the static calculations of point defect energies performed by energy minimization for NiO.[1] In the present work we investigate by molecular dynamics the GB diffusion in an oxide that has the NaCl structure and we have chosen to study the migration mechanism of a cationic vacancy in nickel oxide.

Experimental studies of grain-boundary diffusion in nickel oxide have been carried out in polycrystalline materials as well as in bicrystals. The results are somewhat contradictory as far as the enhancement of cationic diffusion due to the boundaries is concerned. Some authors have reported an increase of nickel diffusion in grain boundaries of the order of 10^5-10^6.[2,3] However, in other studies the diffusion enhancement is far less important and sometimes it is not even detectable.[4,5] To explain this discrepancy, the role of the impurities has been invoked[4] as well as the preparation technique of the samples.[5] An analogous controversy exists also for cobalt diffusion in grain boundaries of NiO.[5–8]

Nickel oxide is slightly nonstoichiometric with a deficiency in nickel and the majority of the defects are cation vacancies. These vacancies are doubly or singly charged, their relative percentage being a function of the temperature and of the partial oxygen pressure. Farhi and Petot-Ervas[9] have shown that the majority defects are singly charged vacancies at relatively low temperatures and high partial oxygen pressures while doubly charged vacancies predominate at high temperatures and small partial oxygen pressures.

Static computer simulations of anionic and cationic point defects energies have been performed for some tilt grain boundaries of nickel oxide. The outcome of these studies is that there are grain-boundary sites where the creation of defects is more favorable than in the bulk.[1] Some selected migration paths have been investigated for the nickel vacancy and the oxygen interstitial. The calculated activation energies are lower than that of the volume.[10,11] However, as mentioned by the authors, these studies have some limitations due to the use of static methods. First, all the possible diffusion paths have not been studied and, second, no temperature effect has been taken into account.

In this study, the molecular-dynamics (MD) method is used to investigate the diffusion of a nickel vacancy in a NiO GB. With this method it is possible to overcome some of the previous limitations since there is no assumption for the diffusion paths and because the system can be studied as a function of the temperature. The analysis of the atomic trajectories obtained by MD gives a detailed description of the microscopic mechanisms of grain-boundary diffusion and allows one to calculate directly the related quantities, such as the diffusion coefficient and the migration energy of the defect.

We have chosen to study a $\Sigma5(310)[001]$ tilt grain boundary in nickel oxide. The structure of this GB has already been investigated by MD and remains stable up to high temperature.[12] This result has been confirmed by further calculations in which several configurations of this GB, with

and without point defects, have been studied.[13] Some technical reasons related to computer time have also militated in favor of this choice. First, a model related to diffusion data obtained for metallic GB's (Ref. 14) shows that the diffusivity is expected to increase with the boundary angle θ and then to be maximum in a range $\theta=35-55°$ in the case of a [001] tilt axis.[15] The tilt angle (36.9°) of the chosen GB lies in this range. Second, the diffusion studies require long runs in order to obtain a satisfactory accuracy and as a consequence the system size cannot be too large. The $\Sigma5(310)[001]$ GB is characterized by its small periodicity and a small number of atoms per structural unit. This allows us to use a model containing several GB structural units while the total number of atoms remains compatible with a reasonable CPU time.

As is the practice in MD simulations using triperiodic boundary conditions, the vacancy must be introduced in the system. Thus we remove a cation from a GB site in order to create a vacancy. With this procedure, we create a doubly charged point defect. The atomic trajectories produced by MD are analyzed in order to identify the atomic jumps due to the defect diffusion. We then calculate the jump frequencies and the diffusion coefficients of the vacancy as a function of the temperature. The simulations are carried out at high temperature in order to ensure that we have an important number of defect jumps leading to an acceptable statistical error in the calculated quantities.

This paper is organized as follows. In Sec. II we describe the model and the procedures used to calculate the diffusion coefficient of the vacancy. This section also includes the static calculations of the binding energy of the doubly charged nickel vacancy for several sites of the grain boundary. In Sec. III we present the results concerning the study of vacancy diffusion in the grain boundary as a function of temperature. The technique employed to analyze the migration jumps of the vacancy is described. We also calculate the residence time at the most visited sites and the migration energies related with these particular sites. The GB diffusion coefficients of the vacancy computed at every studied temperature are plotted on an Arrhenius graph and the migration energy is obtained from a linear fitting. The nickel vacancy diffusion in the bulk is investigated in order to evaluate the GB diffusion enhancement as a function of the temperature. The bulk and GB migration energies are used in combination with the binding energies of the vacancy to calculate the nickel diffusion enhancement at the boundary. This result is compared with the available experimental results. In the last section we present some concluding remarks resulting from the present work.

II. MODEL AND COMPUTATIONAL DETAILS

The MD simulations have been carried out in the NVT ensemble (constant number of particles, volume, and temperature) using Nosé's method.[16] The equations of motion are integrated with a time step $\delta t=1$ fs and the pseudomass of Nosé's thermostat has been chosen equal to 10^{-36} erg s^2. In order to describe the atomic interactions we use a rigid ion potential developed for NiO (Ref. 17) and already employed to study the structure of the $\Sigma5(310)[001]$ grain boundary.[12] The short-range interactions are truncated

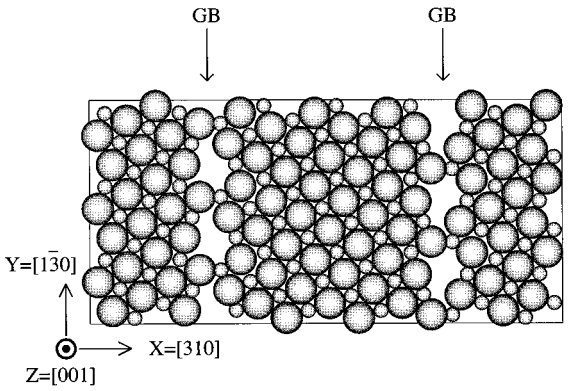

FIG. 1. Schematic drawing of a (001) plane perpendicular to the tilt axis showing the location of the cations (small spheres) and anions (large spheres). The arrows indicate the location of the two GB's. The X, Y, and Z directions are parallel to the edges of the simulation cell. The simulation cell contains 12 (001) planes stacked along the z direction. In two successive planes, the sites are alternatively occupied by cations or anions.

at a cutoff distance $r_c=1.67a$, a being the lattice parameter. The Ewald method is used to calculate Coulomb forces and energy. The convergence parameter for the Ewald summation is $\alpha=5.0/(2r_c)$. The number of reciprocal space vectors $\mathbf{k}$ is given by the following relations: $-5\leqslant n_x,\ n_y,\ n_z\leqslant5$ and $0<n_x^2+n_y^2+n_z^2\leqslant27$, where n_x,n_y,n_z are the integers defining the components of the $\mathbf{k}$ vectors: $\mathbf{k}=2\pi(n_x/L_x,n_y/L_y,n_z/L_z)$, L_x,L_y,L_z being the dimensions of the simulation box. In order to obtain the temperature dependence of a, we have performed preliminary MD simulations on a perfect crystal in the range $T=1500-2700$ K and at each temperature the lattice parameter a has been fitted to give a practically zero pressure. In order to evaluate the melting temperature of our model we have simulated a system with free surfaces and found that the melting occurred rather rapidly at $T=3050$ K. On the other hand the simulations performed on the GB do not show any instability up to a temperature of $T=2800$ K. Thus we can conclude that with our model potential the system remains solid and stable in the temperature range (2250–2650 K) used for the diffusion study.

The simulation box containing the $\Sigma5(310)[001]$ GB is a parallelepiped with edges parallel to the directions x:[310], y:[1$\bar{3}$0], and z:[001]. The simulated system contains 12 (001) planes stacked in the z direction. This results in a total of 2160 ions (1080 cations and 1080 anions). Periodic boundary conditions are applied in the three directions x,y,z, and they generate a second grain boundary in the system as shown in Fig. 1, where the atoms belonging to a (001) plane of the system are drawn. The dimensions L_x, L_y, and L_z of the simulation cell at $T=0$ K are equal to 41.89, 19.77, and 25.01 Å, respectively. They vary with temperature as a function of the lattice parameter a. The value of L_x corresponds to a distance between the GB's equal to $3a$[310]; it is large enough to avoid boundary interactions. Indeed there is a region between the GB's where the properties are very close to the bulk ones. This has been verified by the calculation of the nearest-neighbor distances.[13]

We have also computed the diffusion properties of a

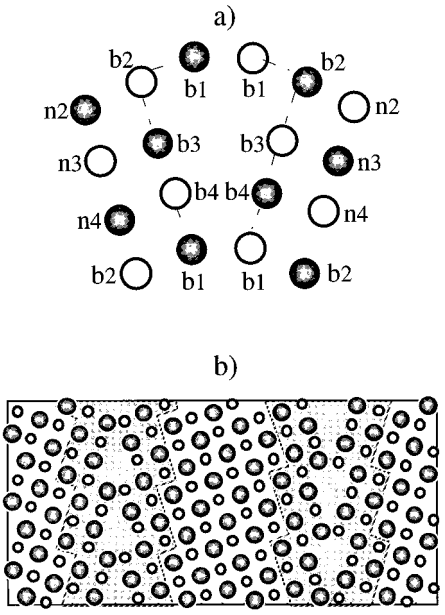

FIG. 2. (a) Projection onto a (001) plane of the cation sites belonging to a structural unit of the $\Sigma 5$ GB. The sites of two successive planes are taken into account. The filled circles correspond to the cations located in the upper plane while the open circles correspond to the lower plane. The b sites are located on the GB planes, the n sites correspond to the ions that have nearest neighbors in the boundary plane. (b) same as Fig. 1; the shaded area containing all the b and n sites is assumed to be the GB region.

nickel vacancy in a perfect crystal and calculated the bulk diffusion coefficient. The simulation cell we use has the same axis orientations and contains the same number of atoms as the model employed in the GB study.

The technical details of our computations are as follows. In a first step we perform static calculations ($T=0$ K) and minimize the energy of the system with a quasidynamical method[18] in order to obtain a relaxed atomic configuration. This configuration is then heated step by step using Nosé's method in order to reach the desired temperature. The temperature difference between two successive steps is equal to 100 K for $T<500$ K and to 150 K for the higher temperatures. Each heating step is performed by MD during 2 ps. The lattice parameter is changed at each heating step. Once the final temperature is attained we perform a longer MD run during 30 ps in order to reach an equilibrium configuration. Next, we introduce two nickel vacancies in the system by extracting, in one structural unit of each GB, a cation from a site defined as $b3$ in Fig. 2(a). A further 30-ps run is performed to stabilize the system before starting the production runs. The duration of the runs varies between 270 and 300 ps and they are carried out at 2250, 2350, 2500, and 2650 K. In the case of the perfect crystal we follow the same procedure of heating but there is only one vacancy introduced in the system. The presence of this single defect combined with the fact that diffusion is slower in the volume requires longer runs ranging from 420 to 600 ps. They are performed at the following temperatures: 2350, 2500, and 2650 K.

The introduction of a cation vacancy results in a net charge in the simulation cell. This problem of a net charge associated to point defects has already been treated by Leslie and Gillan[19] who have given a correction term for the energy calculations. To evaluate this correction term they assume a compensating uniform background charge density and show that this assumption is correct by performing calculations in several test cases. This correction does not depend on the ion positions and thus does not affect the interatomic forces; we have therefore calculated the forces using the usual Ewald method.

TABLE I. Binding energies E^b of the vacancy calculated for different sites of the boundary (see Fig. 2 for definition of the sites).

Site	$b3$	$n2$	$n4$	$b4$	$n3$	$b2$	$b1$
E^b (eV)	-0.31	-0.21	-0.14	0.03	0.44	0.87	3.21

A. Energy of defects

We have calculated the creation energy of a vacancy on the GB sites and in a perfect crystal. In order to calculate the creation energies E^f we use the supercell approach[19] and relax the atomic positions with the quasidynamical method. The results of these computations are used to calculate the binding energy E^b of the vacancy with the GB. E^b is defined by the relation $E^b=E^f_{\mathrm{GB}}-E^f_{\mathrm{bulk}}$, where E^f_{GB} is the energy of creation at the boundary and E^f_{bulk} is the energy of creation in the bulk (perfect crystal). We must mention here that the creation energy of the defect calculated in this context is not directly comparable to the experimental values of the formation energy. In order to obtain this energy one has to take into account the whole oxidation cycle necessary to create a doubly charged cation vacancy (see, for example, Ref. 11).

The binding energies of the cationic vacancies are calculated for several sites of the boundary. We have chosen to restrict the calculation of E^b to the sites drawn in Fig. 2(a). These sites are classified into two categories: the positions of the first sites are at the boundary (b sites), the second ones have neighbors located at the boundary (n sites). The binding energies calculated for the nickel vacancy are listed in Table I. The negative values correspond to sites where the formation of the vacancy is more probable than in the bulk. Such a situation occurs for the $b3$, $n2$, and $n4$ sites, the $b3$ site being the most favorable one. The other sites present positive binding energies, which means that they are not privileged sites with reference to the bulk. The least favorable energy corresponds to the $b1$ site.

Duffy and Tasker[1] have also calculated the binding energies of a nickel vacancy on GB sites by energy minimization. A detailed comparison of the results is not easy since they do not mention the localization of the sites for which their calculation has been performed. The lowest energy they have found is equal to -0.36 eV and comparable to our minimum value (-0.31 eV). Their maximum value (0.88 eV) is significantly smaller than the one we have found (3.21 eV), but it is not clear if they did calculate the binding energy for the $b1$ site. If we do not consider this site, our maximum value is 0.87 eV, which is very similar to their result. This possible agreement is interesting given that we are using different interatomic potentials.

B. Diffusion

The GB diffusion models generally assume that the enhancement of the diffusion coefficient occurs in a region that has the shape of a slab parallel to the GB. The thickness of this slab is considered as the grain-boundary width. In our model, this GB region is the slab that contains the sites labeled in Fig. 2(a). The shaded area of Fig. 2(b) shows the section of this slab with a (001) plane. This definition of the GB region is justified for several reasons. It contains several sites that have a negative binding energy and, in addition, as we shall see in Sec. III A, the migration path of the vacancy will mainly proceed through some sites of this region. The average width of this slab is 10 Å; this is comparable to the grain-boundary width of 7 Å deduced from diffusion experiments in NiO.[2]

The grain-boundary region being anisotropic, we have calculated the components D_z and D_y of the diffusion coefficient in the z and y directions parallel to the grain boundary plane. These components correspond, respectively, to the diffusion parallel to the tilt axis, $D_{\parallel}=D_z$, and perpendicular to it, $D_{\perp}=D_y$. We have also calculated the average diffusion coefficient in the boundary plane $D=(D_{\perp}+D_{\parallel})/2$. In the case of a perfect crystal, where isotropic behavior is expected, the diffusion coefficient has been calculated along the three crystallographic directions [100], [010], and [001].

The migration of simple defects such as vacancies generally occurs via jumps to nearest-neighbor sites. The diffusion coefficient of the defect in a given direction α can be expressed as a function of the frequencies Γ_i and the lengths $d_{i\alpha}$ of the different types of jumps:[20]

$$D_{\alpha}^{\mathrm{def}}=\frac{1}{2}\sum_i \Gamma_i d_{i\alpha}^2. \tag{1}$$

To perform this calculation of D^{def}, it is necessary to identify the different types of jumps and to calculate their frequencies. These results are obtained by the analysis of the atomic trajectories produced by MD.

In the GB region of our model (see Fig. 2) it is possible to define five kinds of jumps according to their contribution in the directions x, y, and z. These five jumps are plotted schematically in a structural unit; the generic names we have chosen to identify these jumps are indicated in Fig. 3 (P stands for in plane jumps, HP for out of plane jumps, and TT is a particular out of plane jumps which connects two sites of the same type). The TT jump can only occur between $b1$ sites and it is the only type of jump involving equivalent sites. The other kinds of jumps occur between nonequivalent sites and may involve different pairs of sites. For instance, the $P1$ jump in Fig. 3 connects $b1$ and $n4$ but it may also occur between the following pairs of sites: $b4$ and $n3$, $b3$ and $n2$. The lengths of these jumps are given in Table II. We see that the jumps that can contribute to the diffusion along the tilt axis (direction $z=[001]$) are HP1, HP2, and TT. The TT jumps are the only ones that do not contribute to the diffusion perpendicular to the tilt axis (direction $y=[130]$). The lengths of the jumps presented in Table II correspond to the ideal distances between the atoms of a geometric configuration (without relaxation), where the expansion perpendicular to the boundary is taken into account. This choice has been done for two reasons: (i) the relaxed positions of the atoms are just slightly modified with reference to the geometric ones. If we considered the relaxed positions we should define many types of jumps and the analysis would be far more complicated; (ii) at high temperature the amplitude of the atomic vibrations is large and the fluctuations of the interatomic distances are higher than the differences between geometric and relaxed positions.

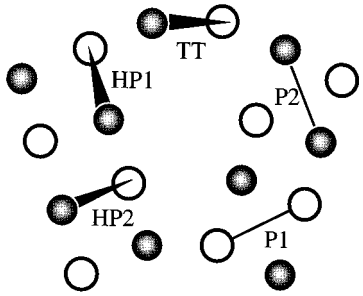

FIG. 3. Same structural unit as in Fig. 2(a). The different types of jumps between nearest-neighbor cation sites in the GB region are drawn. TT, HP1, and HP2 jumps concern sites belonging to the two successive planes. $P1$ and $P2$ jumps occur without change of plane. There is only one jump of each type drawn.

In order to identify the jumps of the defect we select all the atoms that are displaced from their average locations. We have used several criteria for the displacement length and finally we have chosen a value equal to $0.67d_0$ where d_0 is the nearest-neighbor distance between cations. Then a graphical analysis of the selected atoms trajectories allows us to determine if a jump has effectively occurred. We assume that a jump has been performed when, after a displacement larger than the distance criterion, the atom spends a long enough time in its new position. This time limit has been fixed to 3 ps.

To study the bulk diffusion in a perfect crystal we use the same analysis as in the GB to identify the jumps. However, in this case we calculate the vacancy diffusion coefficient

TABLE II. Lengths d_x, d_y, d_z, of the five types of jumps defined in Fig. 3. They are given along the three directions $x[310], y[130], z[001]$ in units of lattice parameter, a.

Type of jump	d_x (a)	d_y (a)	d_z (a)
HP1	$\frac{1}{2\sqrt{10}}$	$\frac{3}{2\sqrt{10}}$	0.5
HP2	$\frac{3}{2\sqrt{10}}$	$\frac{1}{2\sqrt{10}}$	0.5
$P1$	$\frac{2}{\sqrt{10}}$	$\frac{1}{\sqrt{10}}$	0
$P2$	$\frac{1}{\sqrt{10}}$	$\frac{2}{\sqrt{10}}$	0
TT	$\frac{1.3885^a}{\sqrt{10}}$	0	0.5

[a]This length takes into account the distance between the grains calculated by energy minimization.

along the three principal crystallographic directions [100], [010], and [001]. All the sites are equivalent and of course there are no TT jumps.

In the case of the grain boundary we only take into account the jumps involving the sites of the boundary region while for the perfect crystal all the jumps are taken into account.

At present we have only discussed the diffusion coefficient of a defect but the quantity measured experimentally is the atomic diffusion coefficient. This coefficient also includes the defect concentrations and the correlation factors that are characteristic of each diffusion mechanism. The atomic diffusion coefficient D^{atom} is obtained by summing up the contributions of the different defect mechanisms.[20] D^{atom} calculated in the α direction is given by

$$D_{\alpha}^{\mathrm{atom}}=\sum f_{\alpha}^{\mathrm{def}} C^{\mathrm{def}} D_{\alpha}^{\mathrm{def}}, \tag{2}$$

where $f_{\alpha}^{\mathrm{def}}$ is the correlation factor and C^{def} is the corresponding defect concentration.

In MD simulations the atomic diffusion coefficient can also be directly obtained from the mean-square displacement $\langle \delta r^2(t)\rangle = \langle [\mathbf{r}(t)-\mathbf{r}(0)]^2\rangle$ of the atoms. In order to evaluate the GB atomic diffusion coefficient, we have calculated the mean-square displacement of the atoms belonging to the GB region. These computations are performed for the two directions parallel to the tilt axis $[\langle \delta z^2(t)\rangle]$ and perpendicular to it $[\langle \delta y^2(t)\rangle]$. From the slope of the linear parts of $\langle \delta z^2(t)\rangle$ and $\langle \delta y^2(t)\rangle$ we deduce the nickel diffusion coefficient for each direction using the relation

$$D_{\alpha}^{\mathrm{atom}}=\frac{1}{2t}\langle \delta r_{\alpha}^2(t)\rangle + B_{\alpha}, \tag{3}$$

where B_{α} is a constant.

In order to compare the values of $D_{\alpha}^{\mathrm{atom}}$ obtained with Eqs. (2) and (3), we need to calculate the defect concentration in the GB region. This concentration is the ratio between the number $N_{\mathrm{GB}}^{\mathrm{def}}$ of cationic defects in the boundary zone and the number of nickel atoms located in the same region. As we shall see later on, in the case of the GB we may have a spontaneous creation of defects such as Frenkel pairs adding to the vacancies. When the only defects are the two vacancies initially introduced in the system, $N_{\mathrm{GB}}^{\mathrm{def}}$ is not always equal to 2, since these defects may diffuse for a certain time outside the GB zone defined in Fig. 2(b). In fact this behavior has been mainly observed at the two highest temperatures. To obtain the number of defects we calculate the time t_{GB} spent by each defect in the boundary region and $N_{\mathrm{GB}}^{\mathrm{def}}$ is given by

$$N_{\mathrm{GB}}^{\mathrm{def}}=\frac{\Sigma t_{\mathrm{GB}}}{t_{\mathrm{simul}}}, \tag{4}$$

where t_{simul} is the duration of the simulation. When the two initially introduced vacancies spend all the time inside the boundary region, the sum of their t_{GB} times is $\Sigma t_{\mathrm{GB}} = 2t_{\mathrm{simul}}$ and their number is equal to 2.

The defects contained in our simulated system are mainly the cation vacancies created by removing two nickel ions. Consequently the vacancy concentration is imposed to the system and this is not the equilibrium one. The atomic diffusion coefficient obtained in these conditions with Eqs. (2) or (3) is not directly comparable to the experimental one. In order to be able to make this comparison, it would be necessary to calculate the defect equilibrium concentration by performing free-energy computations, which are outside the scope of this study.

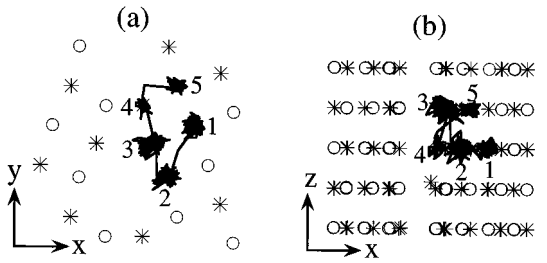

FIG. 4. Partial trajectories projected onto a (001) plane (a), and a (130) plane (b). The trajectories of the atoms displaced by vacancy jumps are plotted. At the beginning the vacancy is located on site 1 and then it jumps successively to sites 2, 3, 4, and 5. Stars and circles correspond to cations and to anions, respectively.

III. RESULTS AND DISCUSSION

The main results of the MD study of the grain-boundary diffusion are (i) the description of the vacancy migration paths and the determination of the residence times on several GB sites, (ii) the cation vacancy diffusion coefficient, (iii) the correlation effects and the diffusion anisotropy, and (iv) the GB diffusion enhancement.

A. Migration path

A quantitative analysis of the migration path requires the identification of the jump types and the determination of the atomic sites visited by the vacancy. To perform these operations we use the site definition of Fig. 2 and the jump nomenclature of Fig. 3. The trajectories of atoms displaced by some successive jumps of a vacancy are plotted in Fig. 4. The numbers indicate (in ascending order) the successive positions of the vacancy. Initially it is situated at 1 on an $n4$ site and then by a $P2$ jump it goes to 2 on a $b3$ site. With a HP1 jump it arrives at 3 on a $b4$ site and with another HP1 jump it goes to 4 on a $b1$ site. From there it jumps via a HP2 jump to 5 on a $b2$ site.

The analysis of the atomic trajectories shows that the vacancy migrates most of the time within the region defined as the boundary zone in Fig. 2. This behavior is illustrated in Fig. 5 where the complete migration paths of the two vacancies at $T=2350$ K are plotted. A comparison of Fig. 5(a) with Fig. 2(b) shows that the majority of jumps have been performed inside the boundary zone. This behavior justifies our *a priori* choice to consider the sites located in this zone as boundary sites. We can also notice in Fig. 5(b) that the vacancy trajectory appears to be elongated in the direction parallel to the tilt axis. Another important feature is that practically all the jumps are nearest-neighbor jumps.

We have calculated, at every studied temperature, the number of jumps belonging to each category. The main result of this calculation is that all the types of jumps are not observed with the same probability; the most frequent ones are TT, $P1$, and HP1. They occur on a restricted number of sites and correspond to $b1$-$b1$, $b1$-$n4$, and $b3$-$b4$ jumps,

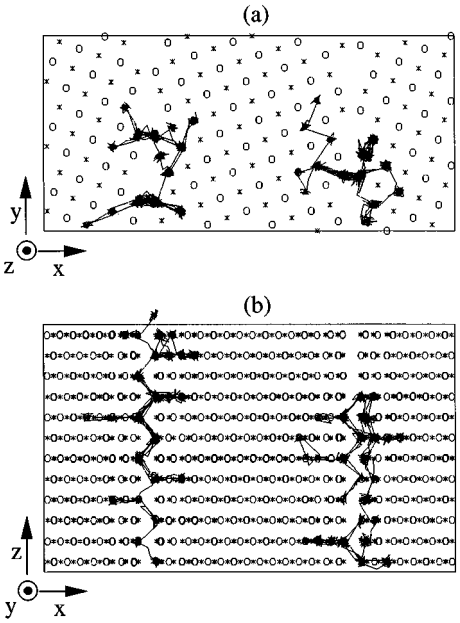

FIG. 5. Trajectory of the cations displaced by vacancy jumps. Projections onto a (001) plane (a) and a (130) plane (b) are shown. Simulation run performed at $T=2350$ K: duration: 300 ps.

respectively. TT jumps between $b1$ sites constitute the major part of the total jumps. In fact their percentage varies between 34% and 43% in the temperature range we studied. The jumps $b1$-$n4$ constitute nearly 20% of the total number of jumps. The percentage of the jumps $b3$-$b4$ varies between 11% and 21%. Other less frequently observed jumps maintain a continuous migration path between the $b1$, $n4$, $b3$, and $b4$ sites.

The categories of sites that are the most frequently visited are in decreasing order: $b1$, $n4$, $b3$, and $b4$. Among them only two ($n4$ and $b3$) have a negative binding energy, while the most frequently visited sites ($b1$) have a formation energy less favorable than in the bulk. The last category of sites ($b4$) has a positive binding energy and is also frequently visited but the trajectory analysis shows that the vacancy leaves these sites as soon as it arrives. On the other hand the $n2$ sites have a negative binding energy and are nearly not visited. These results show clearly that the binding energy criterion is not sufficient to determine the migration path. Of course the energy classification of the GB sites is rigorously valid at $T=0$ K. At finite temperature, the entropy contribution could vary from site to site and the relative probabilities of the presence of the vacancy on each type of site could be modified. Nevertheless the large positive value of E^b for the $b1$ sites is certainly enough to make them the least probable sites. Since these sites are, however, the most visited ones we must conclude that the migration path depends strongly on the dynamic effects.

To give a quantitative description of the GB migration, we have calculated the time spent by the vacancy on each variety of site as well as the number of times they have been visited. This allows us to define an average residence time with the following relation:

$$\tau_{\mathrm{res}}=\frac{t_{\mathrm{life(vac)}}}{N_{\mathrm{visits}}}, \tag{5}$$

TABLE III. Residence time of the vacancy τ_{res} (in ps) on the most frequently visited sites calculated as a function of the temperature.

T (K)	τ_{res} site $b1$	τ_{res} site $n4$	τ_{res} site $b3$
2250	5.5±0.8	16.7±4.8	13.9±4.4
2350	4.5±0.6	10.6±2.7	9.4±3.1
2500	3.9±0.5	7.25±1.8	7.7±1.2
2650	2.9±0.3	6.5±1.4	3.4±0.8

where $t_{\mathrm{life(vac)}}$ is the total time spent by the vacancy on a site of a given type and N_{visits} is the number of times the vacancy has occupied this kind of site.

The values of the residence time calculated for the most frequently visited sites, $b1$, $b3$, and $n4$ are listed in Table III. As expected the average residence time decreases with increasing temperature and we can also notice that it is longer for the two categories of sites characterized by negative binding energies ($b3$ and $n4$).

In the case of a perfect crystal where all the sites are equivalent, the residence time is equal to the inverse of the jump frequency Γ and is consequently related to the migration energy through the relation

$$\tau_{\mathrm{res}}=\frac{1}{\Gamma}=\frac{1}{\Gamma_0}\exp\left(\frac{E^m}{k_BT}\right). \tag{6}$$

For the GB where all the sites are not equivalent, the inverse of the residence time will be equal to the sum of the jump frequencies corresponding to each class of sites.

We have reported the calculated residence times for the three categories of most visited sites in an Arrhenius plot (Fig. 6). For the temperature domain we studied it is possible to adjust a straight line on the variation of $\ln\tau_{\mathrm{res}}$ as a function of $1/k_BT$ and to deduce an activation energy for each category of sites. This energy could be interpreted as an effective migration energy taking into account all the kinds of jumps involving this site. The corresponding effective migra-

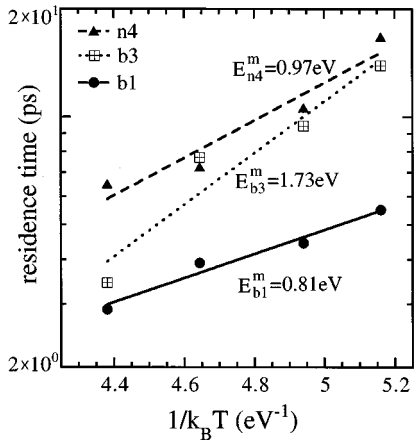

FIG. 6. Arrhenius plot of the residence times of the cation vacancy on GB sites. The calculations have been performed for the most frequently visited sites: $b1$, $b3$, and $n4$. The effective migration energies E^m corresponding to the jumps involving these sites are also indicated.

TABLE IV. Number of jumps N and jump frequencies Γ (in 10^{10} Hz) of the nickel vacancy as a function of temperature. Results concerning the different kinds of jumps involving only nearest neighbors (see Fig. 3). $N_{\parallel}=N_{\mathrm{HP1}}+N_{\mathrm{HP2}}+N_{\mathrm{TT}}$, $N_{\mathrm{tot}}=N_{\parallel}+N_{P1}+N_{P2}$.

T (K)	N_{tot}	$N_{\parallel}$	$N_{\perp}$	Γ_{HP1}	Γ_{HP2}	Γ_{TT}	Γ_{P1}	Γ_{P2}
2250	77	52	44	2.8 ± 0.7	0.3 ± 0.2	5.5 ± 0.9	3.7 ± 0.8	0.5 ± 0.3
2350	92	57	53	3.0 ± 0.8	0.4 ± 0.3	7.4 ± 1.2	4.4 ± 0.9	2.3 ± 0.7
2500	118	84	79	7.3 ± 1.2	1.3 ± 0.5	7.5 ± 1.2	5.2 ± 1.0	1.3 ± 0.5
2650	172	118	98	6.0 ± 1.0	1.8 ± 0.6	13.1 ± 1.5	6.9 ± 1.1	2.6 ± 0.7

tion energies are noted on the plot. We see that the migration energy related to $b1$ sites is the lowest one (0.81 eV), then comes that of $n4$ (0.97 eV), and finally that of $b3$ (1.73 eV).

We further examined the results by analyzing the contribution of the different kinds of jumps for each type of site. The vacancy jumps $b1$-$b1$ constitute 67–73% of the total number of the jumps involving the $b1$ sites. In the case of $n4$ the major contribution results from the jumps $n4$-$b1$ (60–83%) and in the case of $b3$ it comes from the jumps $b3$-$b4$ (55–69%). We can reasonably expect that the major contribution to the effective energy for each type of site will result from the migration energy of the most frequent jump. Consequently, the effective energies (0.81, 0.97, 1.73) can be considered as approximate values of the migration energies of the jumps $b1$-$b1$, $n4$-$b1$, and $b3$-$b4$.

The approximate value of the $b3$-$b4$ jump migration energy is comparable to the result (1.86 eV) obtained by Duffy and Tasker[10] in their static calculation of the same vacancy jump.

The previous results reveal that the mechanisms of migration at the boundary are rather complex. A qualitative analysis of the structural unit geometry shows that the nearest-neighbor environment is different for each type of boundary site. This fact may explain the variation of their frequency of visits. The relative disparity in the sites' environment also varies the energy barriers existing between the neighbor sites. As a result, a limited number of site types associated with the easier jumps only contribute to the diffusion process.

To characterize the migration path we have only taken into account the most frequent jumps occurring between first neighbors. At the higher temperatures investigated (2500 and 2650 K) we have observed other mechanisms and defects such as vacancy jumps to more distant neighbors, cyclic events, and the creation of Frenkel pairs. The first category concerns jumps that are not defined in Fig. 3. They are observed between GB sites located on opposite sides of the boundary plane. Such jumps are $b1$-$b4'$, $b3$-$b3'$, and $b4$-$b4'$ (the prime indicating that the site is situated on the other side of the boundary plane). During the cyclic exchanges, two or more atoms exchange positions during very short times without any creation of a vacancy. We have also observed the spontaneous creation of Frenkel pairs where the interstitials are not particularly mobile in contrast to the corresponding vacancies. The Frenkel pairs are created by the jump of an atom located at the boundary towards the center of the structural unit. These jumps generally lead to a change of plane in the [001] direction. In most cases the interstitial remains localized at this site until it annihilates with a vacancy that arrives at a neighbor site.

B. GB vacancy diffusion coefficient

In order to obtain the diffusion coefficient of the vacancy with Eq. (1) we have counted the number of jumps belonging to each category defined in Fig. 3. Let us recall that in order to compute the jump frequencies we only take into account the time spent by the vacancy in the boundary zone. The time spent outside is sometimes quite significant. In fact the vacancies move in the volume during 16 ps at 2350 K, 80 ps at 2500 K, and 35 ps at 2650 K. The jump frequencies Γ_i of the different kinds of jumps are reported in Table IV together with the total number of jumps N_{tot}. The number of jumps $N_{\parallel}$ that contribute to the diffusion parallel to the tilt axis and the number of jumps $N_{\perp}$ that contribute to the diffusion perpendicular to the tilt axis are also indicated. We notice that $N_{\parallel}$ is slightly higher than $N_{\perp}$. Besides, if we except the $P2$ jumps, which are infrequent, the length of the jumps in the direction parallel to the tilt axis is always larger than in the perpendicular direction. For these two reasons we can reasonably expect an anisotropy in favor of the direction parallel to the tilt axis.

Using Eq. (1) we have calculated the diffusion coefficient of the nickel vacancy for each temperature studied. The calculation also includes the vacancy jumps corresponding to the other mechanisms appearing at higher temperature. These events are not very frequent (less than 5% of the total number of jumps occurring at the highest temperature investigated) and their jump frequencies are not reported in Table IV. The values of the vacancy diffusion coefficient parallel ($D_{\parallel}^{\mathrm{vac}}$) and perpendicular ($D_{\perp}^{\mathrm{vac}}$) to the tilt axis are given in Table V and plotted in the Arrhenius graph of Fig. 7. The migration energies deduced from a linear fitting of $\ln D$ versus $1/k_BT$ are given in Fig. 7. Taking into account the accuracy of the calculations, we see that the migration energies parallel and perpendicular to the tilt axis are the same.

The migration energy deduced from the temperature evolution of the vacancy diffusion coefficient is an effective migration energy that takes into account all the possible jumps. We have already seen in Sec. III A that the migration path mainly involves a limited number of frequently visited sites and that each site is characterized by a predominant type of jump. We note that the average of the migration energies calculated for the most visited sites (1.17 eV) is very close to the effective migration energy of the vacancy. This value (1.26 eV) is different from that obtained in the static calculation performed in the same GB by Duffy and Tasker.[10] This is not surprising since their calculation limited to one type of jump does not take into account the whole migration path.

TABLE V. Nickel vacancy diffusion coefficients parallel and perpendicular to the tilt axis (in 10^{-5} cm^2 s^{-1}) as a function of temperature. Calculation using the jump frequencies (a is the lattice parameter used at each temperature).

T (K)	a (Å)	$D_{\perp}^{vac}$	$D_{\parallel}^{vac}$	D^{vac}	$D_{\parallel}^{vac}/D_{\perp}^{vac}$
2250	4.2728	1.1±0.3	2.0±0.3	1.5±0.3	1.8
2350	4.2793	1.9±0.5	2.5±0.3	2.2±0.4	1.3
2500	4.2892	2.6±0.6	3.8±0.5	3.2±0.5	1.4
2650	4.2989	3.1±0.6	5.1±1.2	4.1±0.9	1.6

C. Nickel diffusion coefficient

The atomic diffusion coefficient for the nickel ions has been calculated in two different ways. In the first one, the computation of the mean-square displacement $\langle \delta r^2(t) \rangle$ allows us to determine the diffusion coefficient $D(r^2)$ with Eq. (3). In the second one, we use the diffusion coefficient of the defect computed with the jump frequencies and Eq. (2) with $f_{\alpha}^{def}=1$ to perform the calculation of $D(\Gamma)$. The comparison of the results obtained in the two different ways is useful to test the consistency of our calculations and it allows us to make an estimation of the correlation effects by calculating the ratio $D(r^2)/D(\Gamma)$. In this context, we take into account all the events contributing to the GB diffusion of the cations and the calculation of $D(\Gamma)$ includes not only the vacancy jumps occurring in the boundary region but also the interstitial jumps. The defect concentration is calculated as discussed in Sec. II. The two sets of atomic diffusion coefficients are listed in Table VI together with their ratios. We notice that they have the same order of magnitude. The values of $D(r^2)$ are always lower than the diffusion coefficients calculated with the jump frequencies. The main reason for this difference is the following. The calculation of $D(\Gamma)$ does not include any correlation effect ($f_{\alpha}^{def}=1$), while the values of $D(r^2)$ implicitly take into account the possible correlation effects. Indeed the observation of the migration path allows us to make such effects evident. When analyzing the atomic trajectories we have noticed that quite often a vacancy that arrives at a $b1$ site performs a series of successive TT jumps. This behavior can be seen in Fig. 8, where among a series of jumps a succession of seven TT hops is visible.

When there is only one mechanism occurring in the diffusion process, the ratio of the atomic diffusion coefficients, $D(r^2)/D(\Gamma)$, can provide an estimate of the correlation factor f_{α}^{def}. This is the case for the two lower studied temperatures (2250 and 2350 K) where there are only nearest-neighbor vacancy jumps. We can see in Table VI that this ratio is slightly lower than the correlation factor of a vacancy mechanism in a perfect fcc crystal (0.78). At higher temperatures it is not possible to use this ratio to estimate the correlation effects because of the presence of other mechanisms. Even though they are not frequent their contributions cannot be neglected since the corresponding correlation factors could differ significantly as is the case for the interstitials. The values of f_{α}^{def} obtained at $T=2250$ and 2350 K can also be compared to the results of the calculations performed in the case of the vacancy diffusion in a $\Sigma=5(310)$ GB of silver.[21] In this study, the correlation factors are calculated in a large temperature range for the two directions parallel and perpendicular to the tilt axis [001]. Our results are obtained at temperatures relatively close to the melting point where the correlation factors calculated by Mishin[21] are almost independent of the diffusion direction and close to 0.52. This value is smaller than our results (0.69, 0.64). This slight difference could fall within the accuracy of our calculations, but it could also be explained by the significant differences existing between the structural unit configurations of Ag and

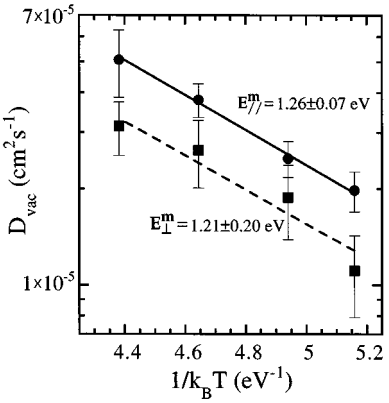

FIG. 7. Arrhenius plot of the vacancy diffusion coefficient in the GB. The diffusion coefficients have been calculated for the directions parallel (continuous line) and perpendicular (dashed line) to the GB tilt axis.

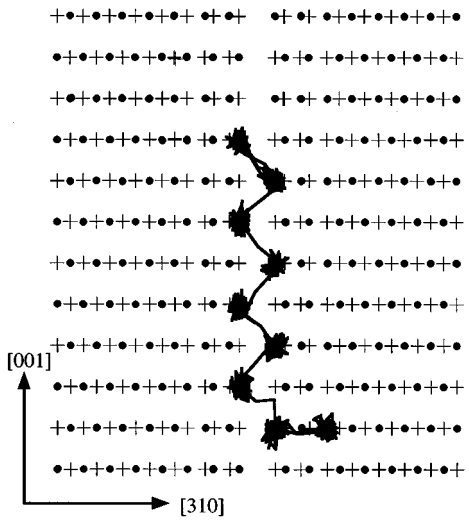

FIG. 8. Cation trajectories showing consecutive TT jumps of the vacancy between $b1$ sites. Projection onto a (130) plane is shown.

TABLE VI. Grain-boundary nickel diffusion coefficients determined from mean-square displacement $D(r^2)$ and from jump frequencies $D(\Gamma)$ (in 10^{-7} cm^2 s^{-1}).

T (K)	$D_{\perp}^{\text{atom}}(r^2)$	$D_{\perp}^{\text{atom}}(\Gamma)$	$D_{\parallel}^{\text{atom}}(r^2)$	$D_{\parallel}^{\text{atom}}(\Gamma)$	$D_{\perp}^{\text{atom}}(r^2)/D_{\perp}^{\text{atom}}(\Gamma)$	$D_{\parallel}^{\text{atom}}(r^2)/D_{\parallel}^{\text{atom}}(\Gamma)$
2250	0.33	0.4 ± 0.1	0.54	0.8 ± 0.1	0.75	0.69
2350	0.46	0.7 ± 0.2	0.60	1.0 ± 0.1	0.64	0.62
2500	0.83	0.9 ± 0.2	1.29	1.3 ± 0.2	0.98	0.98
2650	0.98	1.2 ± 0.2	1.56	1.9 ± 0.4	0.84	0.82

NiO GB's. Consequently the jumps are different and moreover the most frequent one in NiO (TT) does not even exist in silver. Nevertheless we find that the correlation factor does not depend on the diffusion direction; this is in agreement with Mishin's results.

D. Diffusion anisotropy

We have already shown in Sec. III B some evidence of a diffusion anisotropy at the GB. Let us now compare the atomic diffusion coefficients obtained with the two previous approaches. Their ratio $D(r^2)/D(\Gamma)$ calculated for the directions parallel and perpendicular to the tilt axis are reported in Table VI. For a given temperature, the values of the two ratios are very close. This means that the correlation effects are comparable for the two directions. We can thus restrict our discussion of the anisotropy to the results concerning the vacancy diffusion coefficients reported in Table V. We see that the diffusion coefficient parallel to the tilt axis is always higher than the diffusion coefficient perpendicular to it. The value of the anisotropy $D_{\parallel}^{\text{vac}}/D_{\perp}^{\text{vac}}$ varies between 1.3 and 1.8.

There are no experimental results concerning the diffusion anisotropy in grain boundaries of nickel oxide. To our knowledge, the only experimental results available for oxides are those of Stubican and Osenbach.[22] These authors have performed diffusion measurements of ^{51}Cr in several oxides including MgO, which has the same crystalline structure as NiO. They have measured the anisotropy $D_{\parallel}/D_{\perp}$ as a function of the tilt angle of a bicrystal up to 25°. The anisotropy is very high for small angles, and then sharply decreases and reaches a nearly constant value of about 2 for angles higher than 10°. Our results are in qualitative agreement with the experimental ones since we find a small anisotropy value for our high angle grain boundary (36.9°). Besides, our numerical values are close to the experimental limit value of 2.

E. Volume diffusion

We have studied volume vacancy diffusion in order to compare it to the GB diffusion. The total number of jumps calculated at each temperature are reported in Table VII together with the nickel vacancy diffusion coefficients computed for the three ⟨100⟩ directions. As expected for a cubic system, we notice that the diffusion is isotropic within the error limits and the diffusion coefficient of the vacancy is calculated as an average over the three directions. A comparison with the corresponding values obtained for the GB shows that the volume values are lower by nearly a factor of 2. The values of the bulk diffusion coefficients are plotted in an Arrhenius graph (Fig. 9) and give a migration energy for the nickel vacancy equal to 1.54 ± 0.26 eV. As expected, it is higher than the migration energy in the GB (1.26 ± 0.07 eV). This difference will contribute to an enhancement of the nickel diffusion at the grain boundary.

Duffy and Tasker[11] have obtained the migration energy of doubly charged nickel vacancy in the volume by static calculations. Their value (2.5 eV) is significantly higher than ours (1.54 ± 0.26 eV). One possible reason for this difference, apart from the use of different interatomic potentials, may be the fact that at high temperature the atomic vibrations can create local configurations where the energy barriers for migration are lower than those existing at $T=0$ K. These configurations cannot be taken into account in a static calculation.

F. Diffusion enhancement

A plot of the atomic displacements that has some similarity with experimental methods can make evident the existence of a GB diffusion enhancement. All the cations are considered as tracers diffusing from a (001) surface perpendicular to the tilt axis, during diffusion times equal to the duration of the simulations (of the order of 300 ps). We calculate the penetration depth $\Delta z=|z^{\text{fin}}-z^{\text{in}}|$ parallel to the tilt axis $z=[001]$, where z^{in} and z^{fin} are the z atomic coordinates at the beginning and at the end of the simulation run, respectively. We plot Δz as a function of the final position x^{fin} of the cations along the $x=[310]$ axis. The results for the lowest and the highest temperatures we studied are shown in Figs. 10(a) and 10(b), respectively. The displacements Δz of the cations plotted in these figures are larger in the boundary region. In the rest of the system most of the cation displacements are due to thermal vibrations. At the lower tempera-

TABLE VII. Number of jumps and diffusion coefficients (in 10^{-5} cm^2 s^{-1}) of the nickel vacancy as a function of temperature for the perfect crystal.

T (K)	N_{tot}	$D_{[100]}^{\text{vac}}$	$D_{[010]}^{\text{vac}}$	$D_{[001]}^{\text{vac}}$	$D_{\text{tot}}^{\text{vac}}$
2350	33	1.2 ± 0.3	1.05 ± 0.3	0.9 ± 0.3	1.05 ± 0.3
2500	84	2.1 ± 0.4	2.2 ± 0.4	2.45 ± 0.4	2.25 ± 0.4
2650	73	3.0 ± 0.6	2.3 ± 0.5	2.75 ± 0.5	2.7 ± 0.5

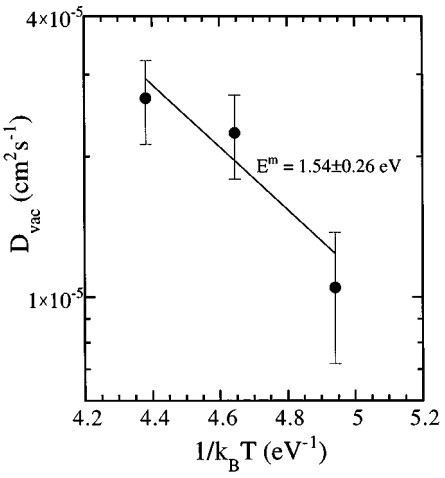

FIG. 9. Arrhenius plot of the bulk diffusion coefficient of the nickel vacancy.

ture the atoms that have diffused are localized in the GB zone while at the higher temperature some bulk diffusion also appears outside this region. Moreover at the highest temperature the displacements in the GB zone are two or three times larger than the ones of the lowest temperature. Given that the duration of the simulation runs is the same, we can also notice that the number of diffusing atoms increases at higher temperature.

In a second part we have used the results of our simulations to calculate an order of magnitude of the diffusion enhancement that is defined as the ratio between the atomic diffusion coefficient at the grain boundary and the atomic diffusion coefficient in the volume. We only take into account the vacancy mechanism and the enhancement ratio is given by

$$R_{\mathrm{GB/Vol}}=\frac{D_{\mathrm{GB}}^{\mathrm{Ni}}}{D_{\mathrm{Vol}}^{\mathrm{Ni}}}=\frac{f_{\mathrm{GB}}^{\mathrm{vac}}C_{\mathrm{GB}}^{\mathrm{vac}}D_{\mathrm{GB}}^{\mathrm{vac}}}{f_{\mathrm{Vol}}^{\mathrm{vac}}C_{\mathrm{Vol}}^{\mathrm{vac}}D_{\mathrm{Vol}}^{\mathrm{vac}}}, \tag{7}$$

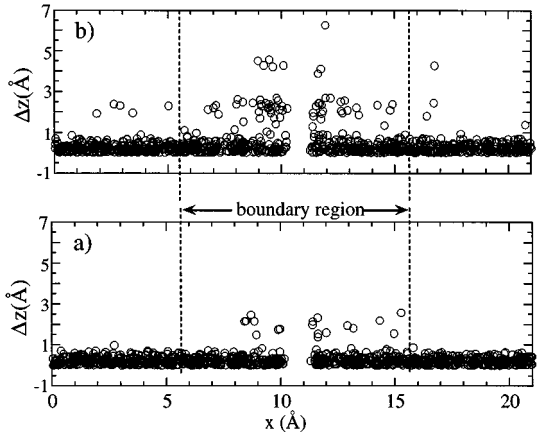

FIG. 10. Total displacement Δz in the z direction of the cations at the end of a run performed during 300 ps at (a) 2250 K and (b) 2650 K. $\Delta z=|z^{\mathrm{fin}}-z^{\mathrm{in}}|$; z^{in} and z^{fin} are the values of the z coordinate at the beginning and at the end of the run. Δz is plotted as a function of the final atomic position x^{fin} in the direction perpendicular to the GB plane.

where $f_{\mathrm{GB}}^{\mathrm{vac}}$ and $f_{\mathrm{Vol}}^{\mathrm{vac}}$, $C_{\mathrm{GB}}^{\mathrm{vac}}$, and $C_{\mathrm{Vol}}^{\mathrm{vac}}$, and $D_{\mathrm{GB}}^{\mathrm{vac}}$ and $D_{\mathrm{Vol}}^{\mathrm{vac}}$ are the correlation factors, the concentrations of the nickel vacancies and the nickel vacancy diffusion coefficients in the GB and in the volume, respectively.

The results reported in Tables V and VII are used to calculate the ratio of the vacancy diffusion coefficients and one gets:

$$\frac{D_{\mathrm{GB}}^{\mathrm{vac}}}{D_{\mathrm{Vol}}^{\mathrm{vac}}}=0.51\ \exp\left(\frac{0.28\ \mathrm{eV}}{k_BT}\right). \tag{8}$$

We can reasonably assume that the ratio of the correlation factors is close to one, since we have seen in Sec. III C that the estimate value in the GB is only a little lower than that for the volume.

In order to calculate the concentration ratio we take into account the fact that the various sites of the grain boundary region are not equivalent and are characterized by different vacancy creation energies. The vacancy concentration at the GB is given by

$$C_{\mathrm{GB}}^{\mathrm{vac}}=\sum_i\ \exp\left(-\frac{E_{\mathrm{GB}}^{f_i}-TS_{\mathrm{GB}}^{f_i}}{k_BT}\right), \tag{9}$$

where $E_{\mathrm{GB}}^{f_i}$ and $S_{\mathrm{GB}}^{f_i}$ are the vacancy formation energies and entropies, respectively. As we restrict ourselves to the calculation of an order of magnitude of the enhancement we neglect the entropy effects. This reduces the ratio of concentrations to

$$\frac{C_{\mathrm{GB}}^{\mathrm{vac}}}{C_{\mathrm{Vol}}^{\mathrm{vac}}}=\sum_i\ \exp\left(-\frac{E_{\mathrm{GB}}^{f_i}-E_{\mathrm{Vol}}^{f}}{k_BT}\right)=\sum_i\ \exp\left(-\frac{E^{b_i}}{k_BT}\right), \tag{10}$$

where E^{b_i} are the binding energies of the vacancy for the different GB site categories. We use the values computed at $T=0$ K (Table I) since it is generally assumed that the formation energy does not vary significantly with the temperature. The binding energies sum is calculated for various temperatures. An exponential fit performed on the resulting values allows us to obtain an effective binding energy $\widetilde{E}^b$. The ratio of concentrations is then given by

$$\frac{C_{\mathrm{GB}}^{\mathrm{vac}}}{C_{\mathrm{Vol}}^{\mathrm{vac}}}=A\ \exp\left(-\frac{\widetilde{E}^b}{k_BT}\right)=3.07\ \exp\left(\frac{0.25\ \mathrm{eV}}{k_BT}\right). \tag{11}$$

The combination of Eqs. (8) and (11) gives the ratio between GB and bulk diffusions:

$$R_{\mathrm{GB/Vol}}=1.57\ \exp\left(\frac{0.53\ \mathrm{eV}}{k_BT}\right). \tag{12}$$

The diffusion enhancement calculated in the temperature range of the experimental work of Atkinson and Taylor[2] is of the order of 10^3. This result is significantly lower than the experimental one (of the order of 10^6) but we must notice that the experiments have been carried out in a polycrystalline material, where there is a large variety of grain boundaries with probably quite different contributions to defect concentration and migration. In the same temperature range there exist results for bicrystals obtained by Barbier *et al.*[5] These authors have not observed any enhancement and they

deduce that if there is any it will be at a maximum of the order of 10^3 (limit of their measurements). This is comparable with our result, but this agreement has to be considered with caution.

Another possible explanation for the difference with the experimental results obtained by Atkinson and Taylor could be the charge state of the vacancy. As we have already mentioned, Farhi and Petot-Ervas[9] have studied single crystals and shown that there are two types of nickel vacancies, singly charged and doubly charged. The relative concentrations of these defects vary with the temperature and the partial oxygen pressure. If these results also apply in the case of grain boundaries, then the Atkinson and Taylor's results have been obtained in conditions where the majority defects are singly charged vacancies. In this study we have investigated the diffusion of doubly charged vacancies, which are majority defects at high temperature and small partial oxygen pressure. The contribution of these two defects to diffusion may be quite different. Such behavior is suggested by the static calculations of Rabier, Soullard, and Puls[23] performed in NiO for a perfect crystal and for an edge dislocation. These authors have found that, in a perfect crystal, the activation energy of the singly charged vacancies is slightly lower than that of the doubly charged vacancies and it is much lower in the case of a dislocation. However, they have investigated a limited number of migration paths and we have shown in the present MD study of a vacancy migration at a GB that the results obtained with static calculations may be not fully representative. An MD study of diffusion of singly charged vacancies could provide more insight into this question. But the simple rigid ion model we have used is not suitable for such a study, which would require one to take into account the electronic freedom degrees in the MD simulation.

IV. CONCLUSIONS

A $\Sigma 5(310)[001]$ tilt grain boundary of NiO has been used to investigate by molecular dynamics the GB vacancy diffusion mechanism in a crystal with NaCl structure. The defect introduced in the simulated system is a doubly charged nickel vacancy and the diffusion of this defect has also been studied in a perfect crystal of NiO. The migration mechanism in the GB is rather complex; all the GB sites are not equivalent as is the case in the bulk diffusion and they are consequently not visited by the defect with the same frequency. The migration path of the vacancy mainly includes some specific sites of the boundary. The temperature dependence of the residence times on the most frequently visited sites shows that it is possible to determine an activation energy for each site. These energies characterize the majority jumps associated to each site. The frequency of a visit does not vary in the same way as the vacancy formation energy and the most visited site even has a positive binding energy with the boundary. This shows that the migration paths mainly depend on dynamical effects, and for this reason molecular-dynamic simulations are more suitable than static calculations to study the GB diffusion mechanisms.

The comparison of the diffusion coefficients calculated in the GB plane shows clearly the existence of a slight anisotropy. The diffusion coefficient of the vacancy is higher in the direction parallel to the tilt axis than in the perpendicular one. This anisotropy is consistent with the experimental results available for other oxides.

The migration energy deduced from the temperature dependence of the vacancy diffusion coefficient is, as expected, lower in the GB than in the bulk.

We have made evident qualitatively and quantitatively the enhancement of the diffusion in the GB. The numerical values are lower than the values deduced from experiments performed in polycrystalline NiO. Our values are apparently in better agreement with the results of other experiments performed in bicrystals.

ACKNOWLEDGMENT

This study has been supported by the scientific council of IDRIS/CNRS (France) through the allocation of computer time (Project CP9/940127).

[1] D. M. Duffy and P. W. Tasker, Philos. Mag. A **50**, 143 (1984).
[2] A. Atkinson and R. I. Taylor, Philos. Mag. A **43**, 979 (1981).
[3] E. G. Moya, G. Deyme, and F. Moya, Scr. Metall. Mater. **24**, 2447 (1990).
[4] A. Atkinson, D. P. Moon, D. W. Smart, and R. I. Taylor, J. Mater. Sci. **21**, 1747 (1986).
[5] F. Barbier and M. Déchamps, J. Phys. (Paris) Colloq. **49**, C5-575 (1988).
[6] A. Atkinson and R. I. Taylor, Philos. Mag. A **45**, 583 (1982).
[7] W. K. Chen and N. L. Peterson, J. Am. Ceram. Soc. **63**, 566 (1980).
[8] F. Barbier, C. Monty, and M. Déchamps, Philos. Mag. A **58**, 457 (1988).
[9] R. Farhi and G. Petot-Ervas, J. Phys. Chem. Solids **39**, 1175 (1978).
[10] D. M. Duffy and P. W. Tasker, J. Phys. (Paris) Colloq. **46**, C4-185 (1985).
[11] D. M. Duffy and P. W. Tasker, Philos. Mag. A **54**, 759 (1986).
[12] M. Meyer and C. Waldburger, Mater. Sci. Forum **126-128**, 229 (1993).
[13] T. Karakasidis, Ph.D. thesis, University Paris 6 (France), 1995.
[14] D. Turnbull and R. E. Hoffman, Acta Metall. **2**, 419 (1954).
[15] R. W. Balluffi, in *Diffusion in Crystalline Solids*, edited by G. E. Murch and A. S. Nowick (Academic Press, New York, 1984), p. 319.
[16] S. Nosé, Mol. Phys. **52**, 255 (1984).
[17] C. Massobrio and M. Meyer, J. Phys. C **3**, 279 (1991).
[18] J. R. Beeler and G. L. Kulcinski, in *Interatomic Potentials and Simulation of Lattice Defects*, edited by P. C. Gehlen, J. R. Beeler, and R. I. Jaffee (Plenum Press, New York, 1972), p. 735; C. H. Bennett, in *Diffusion in Solids, Recent Developments*, edited by A. S. Nowick and J. J. Burton (Academic Press, New York, 1975), p. 73.

[19] M. Leslie and M. J. Gillan, J. Phys. C **18**, 973 (1985).
[20] J. Philibert, *Diffusion et Transport de Matière Dans les Solides* (Les Editions de Physique, Les Ulis, 1990).
[21] Y. Mishin, Philos. Mag. A **72**, 1589 (1995).
[22] V. S. Stubican and J. W. Osenbach, Solid State Ion. **12**, 375 (1984).
[23] J. Rabier, J. Soullard, and M. P. Puls, Philos. Mag. A **61**, 99 (1990).